Impact of shadow glass transition on crystallization in metallic glass

Zhang, H.R.; Yang, Q.; Wei, S.; Yue, Yuanzheng; Yu, H.B.

Published in:
National Science Open

DOI (link to publication from Publisher):
10.1360/nso/20230064

Publication date:
2024

Document Version
Publisher's PDF, also known as Version of record

RESEARCH ARTICLE

National Science Open
3: 20230064, 2024
https://doi.org/10.1360/nso/20230064

Physics

Impact of shadow glass transition on crystallization in metallic glass

Hui-Ru Zhang[1,#], Qun Yang[1,#], Shuai Wei[2], Yuanzheng Yue[3] & Hai-Bin Yu[1,*]

[1]*Wuhan National High Magnetic Field Center, School of Physics, Huazhong University of Science and Technology, Wuhan 430074, China;*
[2]*Department of Chemistry and iMAT Centre for Integrated Materials Research, Aarhus University, Aarhus 8000, Denmark;*
[3]*Department of Chemistry and Bioscience, Aalborg University, Aalborg 9220, Denmark.*

#Contributed equally to this work.
*Corresponding author (email: haibinyu@hust.edu.cn)

Received 19 October 2023; Revised 8 January 2024; Accepted 9 January 2024; Published online 18 January 2024

Abstract: The stability of glass against crystallization is of importance in practical applications and theoretical understanding of the nature of glass materials. Annealing has complicated influences on glass stability. It induces either delayed or early crystallization, depending on detailed protocols and specific materials. By interrogating the thermal behaviors of twelve metallic glasses (MGs), we find that enhanced stability is correlated to another process: the so-called shadow glass transition and its evolution. Delayed crystallization can be observed when the shadow glass transition is shifted to cross the temperature of crystallization. Concurrently, the shadow glass transition evolves to an enthalpy overshoot. Molecular dynamics simulations support these findings and suggest that the suppressed string-like motion, relating to the shadow glass transition and the enthalpy overshoot, is likely the origin of the postponed nucleation ordering and enhanced glass stability.

Keywords: metallic glass, shadow glass transition, crystallization, glass stability, fast scanning calorimetry

INTRODUCTION

Amorphous materials are ubiquitous around us and are increasingly used in modern technologies. Unlike crystals, they do not have a long-range ordered structure and exist in an energy metastable state [1–4]. Through structural relaxation, they can achieve greater energetic stability and even become thermodynamically stable by undergoing nucleation and crystal growth. These processes greatly affect the physical and chemical properties of the final state of the amorphous materials [5–9].

Over the past decade, developing highly stable amorphous materials has been an important mission in glass research [10,11]. The molecule-by-molecule deposition at appropriately high temperatures represents an elegant method for producing the so-called ultra-stable molecular glasses [12–18]. They exhibit extraordinary thermodynamic and kinetic stability comparable to conventional glass that would be annealed for millions of years [12,19].

Thermal annealing is an indispensable technique for modifying the structure and properties of materials. However, it is widely believed that the incubation time for nucleation in MGs decreases significantly with increasing annealing time [20]. This decrease is attributed to the high mobility atoms that lead to con-

centration fluctuations required for large-scale crystallization [21]. For example, in several Zr-Cu based MGs, micron-scale Cu crystal precipitation and separation would occur even at room temperature storage [22]. On the other hand, enhanced glass stability (with low energy states) has been reported in some glasses. For example, Zhao *et al.* [23] show that a Ce-based MG reaches a stable glassy state stored at room temperature for nearly 18 years. Thus, it is still not clear under what conditions annealing could stabilize the glass rather than result in crystallization.

In a recent work, Cheng *et al.* [24] reported that thermal annealing below T_g in $Ge_{15}Sb_{85}$ phase-change material (PCM) can effectively suppress the intensity of secondary (β) relaxation. It was found that suppression of β relaxation sharply slowed down the crystallization rate, thereby enhancing the stability of the amorphous material. This observation raises interesting questions: Is delayed crystallization specific to certain materials or a general phenomenon? At present, measuring β relaxation for glasses with poor glass-forming ability and stability remains a technical challenge. On the other hand, since β relaxation has been linked to the shadow glass transition by fast heating [25], can one predict the stability of the specific glassy materials from calorimetric features?

In this work, we report that a proper annealing protocol can indeed postpone the devitrification of some MGs with poor thermal stability, but not for MGs with wide supercooled liquid regions. By modulating the so-called shadow glass transition and enthalpy overshoot, we can achieve a delayed crystallization and thus improve the stability of the MGs, i.e., extending the temperature window of the supercooled state. More specifically, a delayed crystallization is realized when the shadow glass transition is tuned via annealing to eclipse the original crystallization temperature.

To set the stage, we briefly recall the calorimetry features of glass materials [26,27]. When a rapidly quenched glass is continuously heated at a constant rate from a low temperature (e.g., room temperature), it exhibits a sub-T_g enthalpy relaxation [8,28–30], as schematically shown in Figure 1A. When the glass is sufficiently annealed at temperatures below T_g, an additional endothermic peak appears before the enthalpy relaxation. This pre-endotherm was first observed in MGs [31], and then in oxide glasses [32], and recently in chalcogenide glasses [33]. It was named as the shadow glass transition [32] (Figure 1B) to distinguish it from the real glass transition. However, the two endotherms have different mechanisms, i.e., the real glass transition is associated with the primary (α) relaxation, whereas the shadow glass transition arises from the secondary (β) relaxation [25,34].

When the annealing degree is further increased, the exothermic enthalpy relaxation peak disappears and the

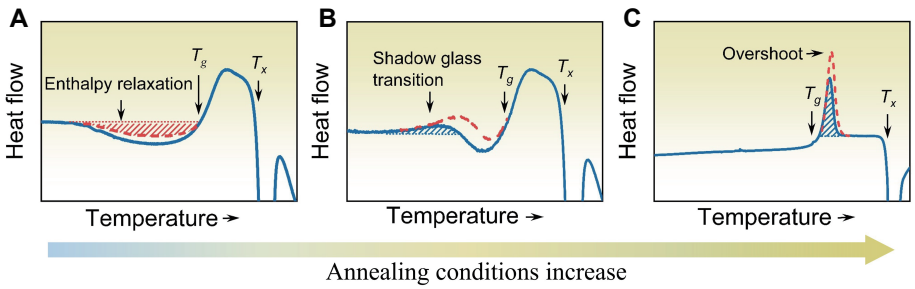

Figure 1 Schematic diagrams illustrating changes in (A) enthalpy relaxation, (B) shadow glass transition, and (C) enthalpy overshoot at the glass transition as annealing conditions increase.

shadow glass transition peak becomes closer to the overshoot of the real glass transition peak, and even overlaps with it [8,35–37], as shown in Figure 1C. If the glass is annealed at T_g for a long time, the overshoot of the glass transition peak will be greatly enhanced.

The features of the shadow glass transition and their underlying mechanisms have been discussed elsewhere [25,32–34], but their structural origins are still not well understood. In this work, we show that the extent of the shadow glass transition can be tailored to promote the stability of glass against devitrification. Revealing the impact of shadow glass transition and glass stability helps our understanding of glass relaxation and glass transition.

RESULTS

Fast scanning calorimetry (FSC) has high temporal resolution and can reach high heating rates (up to 50,000 K/s) [38]. It can characterize and separate weak heat absorption and exotherm signals. Figure 2A shows two FSC upscan curves obtained at 400 K/s for two glass samples with the composition of $Y_{63}Zr_2Cu_{20}Al_{15}$. 400 K/s is a commonly used heating rate in FSC. One sample is the as-cast one, and the other is the one annealed at 563 K for 30 min. The FSC heat flow curves indicate that the as-cast MG crystallizes at T_p = 679 K (peak temperature) immediately after the broad exothermic enthalpy relaxation, while the glass transition does not appear. The annealed MG shows a pronounced enthalpy overshoot before crystallization, with T_p = 688 K. It can be seen that at a heating rate of q = 400 K/s, the crystallization temperature increases by 9 K, i.e., ΔT_p = 9 K.

Next, we annealed the $Y_{63}Zr_2Cu_{20}Al_{15}$ MG for 30 min at different selected temperatures, as shown in Figure 2B. These heat flow curves all have a heating rate of 400 K/s. The as-cast MG shows a large exothermic enthalpy relaxation (see curve A). As the annealing temperature increases, the enthalpy relaxation moves to higher temperatures, and the amount of relaxed enthalpy slowly decreases until it disappears. An additional heat absorption peak (see curves C–I), which is the shadow glass transition, appears before the enthalpy relaxation.

With a higher annealing temperature (curves I–L), the shadow glass transition becomes more pronounced and evolves to an enthalpy overshoot. Curve *L* shows that only the enthalpy overshoot dominates.

We note that the crystallization temperature of curve L is higher than others. Curves A–K have almost the same crystallization temperature, T_p = 679 K. While curve L has T_p = 688 K, the T_p is increased by 9 K. This indicates that annealing at 563 K for 30 min increases the stability of the glass sample. This reinforces the observations of Figure 2A.

Figure 2C displays T_p as a function of log q for both the as-cast and annealed MGs. The annealing condition used for the annealed MG is the same as curve *L* in Figure 2B. T_p values are taken from q = 5 K/s to q = 10,000 K/s, covering five orders of magnitude of the heating rate. The FSC curves, presented in Figure S2, are used to obtain these T_p values. Over a wide range of heating rates, the crystallization temperature of this annealed MG (at 563 K for 30 min) is increased compared to that of as-cast MG. In contrast, for the MG annealed at a lower temperature (e.g., 513 K for 30 min, curve J in Figure 2B), the crystallization temperature has not yet been increased, as shown in the inset of Figure 2C.

Figure 2D shows the crystallization temperature difference between the annealed and the as-cast samples,

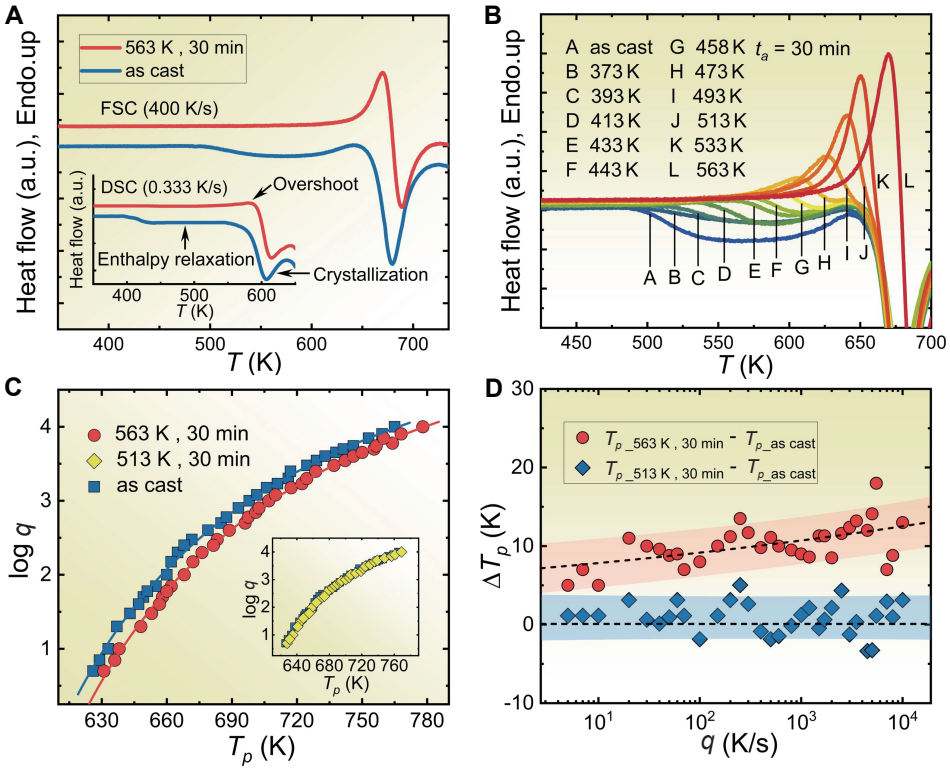

Figure 2 (A) Stabilization of the $Y_{63}Zr_2Cu_{20}Al_{15}$ MG against crystallization through sub-T_g annealing. (B) FSC curves exhibit the effect of annealing at various temperatures T_a for 30 min on the sub-T_g relaxation behavior. The heating rate of those curves is 400 K/s. (C) Plotting the peak temperature of crystallization (T_p) as a function of logarithmic heating rate (log$q$). (D) Temperature difference (ΔT_p) versus heating rate (q). ΔT_p is the difference between the peak crystallization temperature of the annealed and cast samples.

using the same data in Figure 2C. One can see that the increased crystallization temperature is obvious in the sample annealed at 563 K but not in the sample annealed at 513 K.

Under what conditions can we have the crystallization temperature increased? It is interesting to note curve J in Figure 2B that the increased crystallization temperature happens to be observed when the annealing-induced overshoot occurs at the temperature for the original crystallization onset. In the following, we demonstrate this is necessary for postponing crystallization by annealing.

Figure 3 shows the impact of both the heating rate and annealing condition on the crystallization of the MGs. Figure 3A shows the as-cast MG; the shadow glass transition does not appear, and there is only a large exothermic enthalpy relaxation. Even at the high heating rate of the FSC, the glass transition remains unrevealed and crystallizes directly. After annealing at 433 K for 30 min, as shown in Figure 3B, the shadow glass transition appears, the enthalpy relaxation decreases, and exothermic crystallization follows. The crystallization rate under this annealing condition is the same as that of the as-cast MG. After annealing at 563 K for 30 min, as shown in Figure 3C, MG undergoes direct crystallization after a heat-absorbing enthalpy overshoot. At this time, the overshoot exceeded the original crystallization onset temperature and then the crystallization temperature increased.

From Figure 3A–C, we can summarize the condition that annealing can shift crystallization to higher temperatures: when the annealing-induced overshoot exceeds the original crystallization onset temperature.

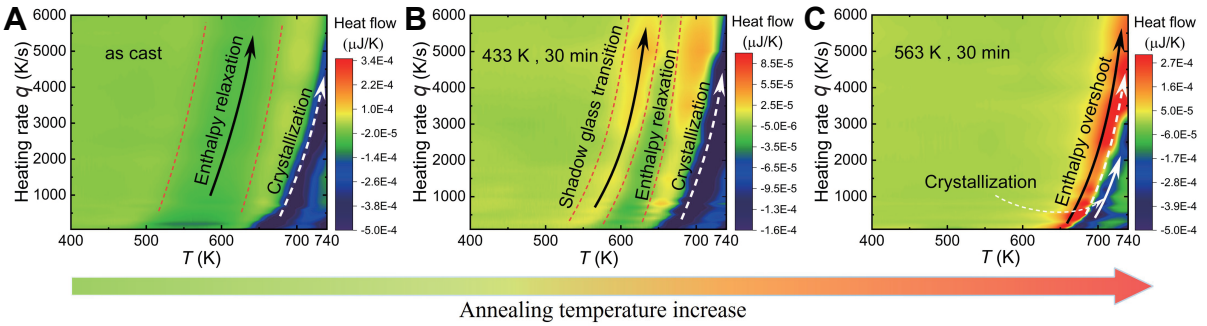

Figure 3 Effects of annealing condition and heating rate on enthalpy relaxation, shadow glass transition, and crystallization for the sample $Y_{63}Zr_2Cu_{20}Al_{15}$ MG. (A), (B), and (C) show the heat flow diagrams of the as-cast sample, the sample annealed at 433 K for 30 min, and the sample annealed at 563 K for 30 min, respectively. They have the same horizontal coordinate, i.e., heating from 400 K to 740 K. The heating rates are both from 100 K/s to 6000 K/s.

Table 1 The composition and thermal properties of the samples are listed[a)]

ID	Composition	T_g (K)	T_p (K)	T_a (K), t_a (h)	ΔT_p (K)
1	$La_{80}Al_{15}Ni_5$	–	463	363, 4	8.5
2	$La_{75}Al_5Ni_{20}$	–	464	383, 4	8
3	$Al_{87}Ni_{10}Ce_3$	–	518	403, 4	7
4	$Y_{65}Co_{35}$	624	703	533, 4	0
5	$La_{60}Al_{20}Ni_{20}$	473	632	403, 4	0
6	$La_{55}Al_{15}Ni_{30}$	487	597	403, 4	0
7	$La_{50}Al_{20}Ni_{30}$	523	623	433, 4	0
8	$La_{50}Al_{10}Ni_{40}$	508	570	413, 4	0
9	$La_{50}Al_{30}Cu_{20}$	518	658	393, 4	0
10	$Al_{86}Ni_{10}Sm_4$	603	636	461, 4	0
11	$Al_{86}Co_9Ce_5$	632	662	543, 4	0
12	$Ce_{55}Ni_{20}Al_{25}$	506	628	393, 4	0
13	$Ge_2Sb_2Te_5$ [33]	–	433	388, 1	4
14	GeSe [33]	568	590	438, 1	0

a) Thermodynamic parameters of different MGs obtained by FSC at a heating rate of 400 K/s. T_g and T_p are the glass transition temperature and peak crystallization temperature of the as-cast sample, respectively. T_a and t_a are the annealing temperature and annealing time, respectively. ΔT_p indicates the difference in peak crystallization temperature before and after annealing.

We have shown increased crystallization temperatures after annealing in $Y_{63}Zr_2Cu_{20}Al_{15}$ MG. This MG has poor thermal stability. Therefore, it is of interest to investigate MGs with relatively good thermal stability to understand the effect of annealing on the crystallization kinetics of MGs.

We measured twelve MGs listed in Table 1. Figure 4 corresponds to the heat flow curves of some MGs as examples. The heating rate is 400 K/s. The annealing temperatures for these MGs are chosen to be $0.75T_p$–$0.9T_g$ ($0.75T_p$–$0.9T_p$ for MGs that do not reveal the glass transition). We find that three MGs, $La_{80}Al_{15}Ni_5$, $La_{75}Al_5Ni_{20}$, and $Al_{87}Ni_{10}Ce_3$, show a similar increase in crystallization temperatures as for $Y_{63}Zr_2Cu_{20}Al_{15}$ after annealing. All of them do not reveal the glass transition either by DSC or FSC (400 K/s).

On the other hand, the other nine (Nos. 4–12) MGs exhibit the glass transition at 400 K/s by FSC. These glasses show a large overshoot at the glass transition after annealing. The overshoot neither crosses over the supercooled liquid region nor affects the crystallization rate. Two typical examples are shown in Figure 4C and D. Thus, we have observed the impacts of shadow glass transition and overshoot on the stability of

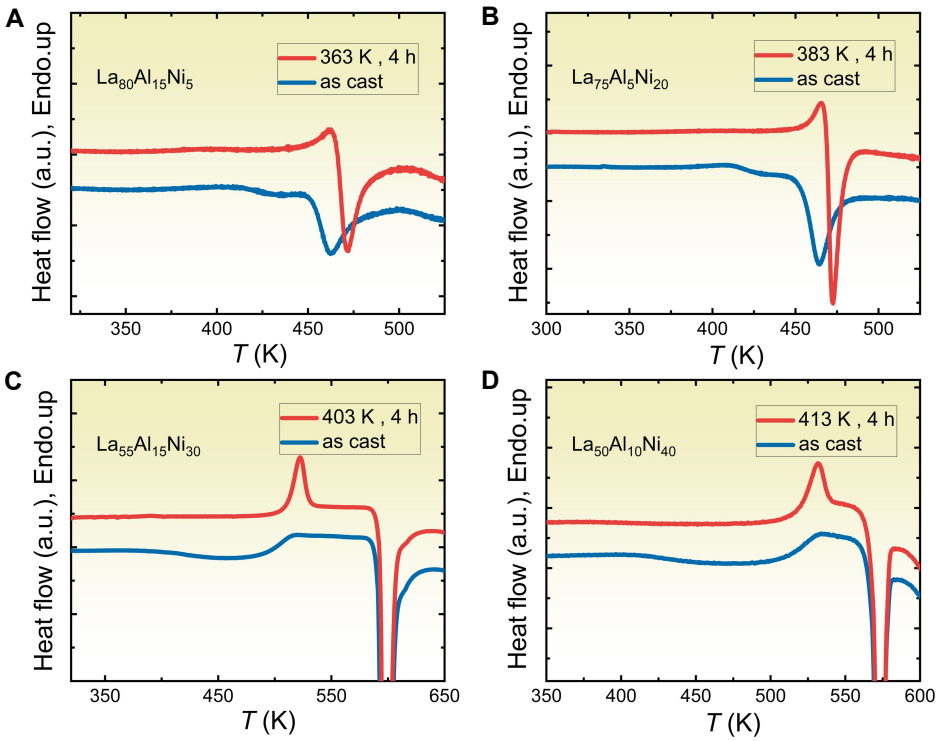

Figure 4 Heat flow curves of $La_{55}Al_{15}Ni_{30}$ and $La_{50}Al_{10}Ni_{40}$ MGs with a heating rate of 400 K/s. Each MG is compared for crystallization in the as-cast state and under the corresponding annealing conditions.

metallic glasses.

We used an isothermal program to characterize the crystallization rate of MGs, as shown in Figure 5A. First, the sample is heated from room temperature to a preset temperature T_q at a high heating rate of 3000 K/s. Such a high heating rate is used to ensure that the signal of the speed of crystallization can be amplified. Then, the sample is held at that temperature for 10 s, and the FSC signal of the process is recorded; the time required to reach the maximum rate of crystallization is obtained. Finally, the temperature returns to room temperature at a cooling rate of 100 K/s.

Different T_q values are selected for multiple measurements in the experiments. Figures 5B–F correspond one by one to Figures 2A, 4A–D for $Y_{63}Zr_2Cu_{20}Al_{15}$, $La_{80}Al_{15}Ni_5$, $La_{75}Al_5Ni_{20}$, $La_{55}Al_{15}Ni_{30}$, and $La_{50}Al_{10}Ni_{40}$, respectively. It can be observed that for samples in Figure 5B–D, the lower the isothermal temperature is, the more pronounced the crystallization delay is. In contrast, for samples Figure 5E and F, the crystallization speed is constant at any isothermal temperature.

DISCUSSION

These results suggest that for these MGs with poor thermal stability, the underlying cause of the delayed crystallization is related to the shadow glass transition and enthalpy overshoot. As the annealing conditions increase, the shadow glass transition starts to appear and moves toward crystallization, which evolves into an

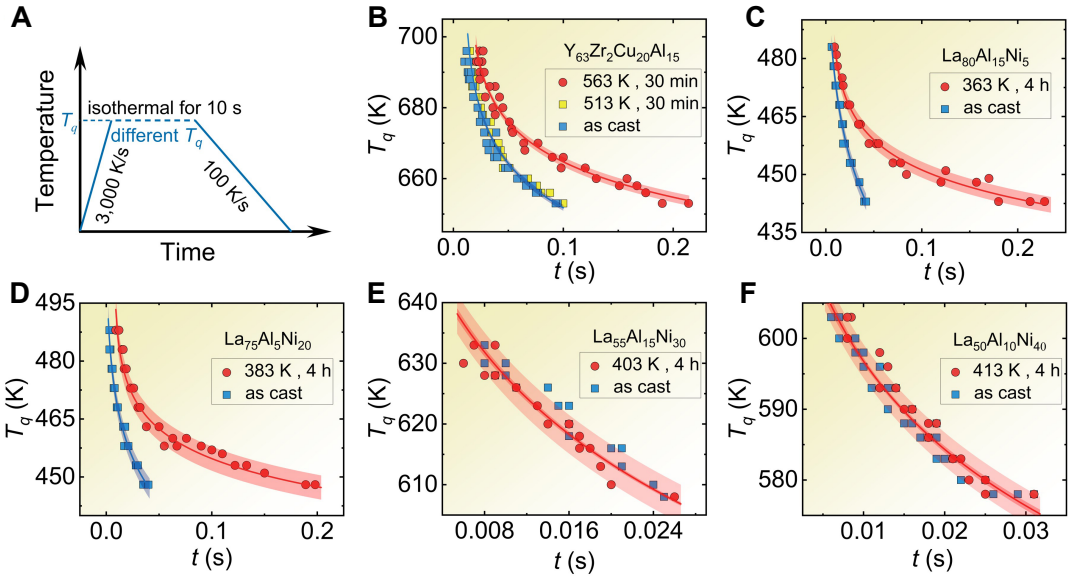

Figure 5 (A) The diagram of FSC experimental steps. T_q is a certain preset temperature that is lower than T_x (crystallization onset temperature). Isothermal at this preset temperature for 10 s to obtain the time (t) needed for crystallization, usually $t < 10$ s, because T_q is chosen high enough. (B)–(F) T_q versus t of five different MGs. Each MG is compared in both annealed and as-cast states.

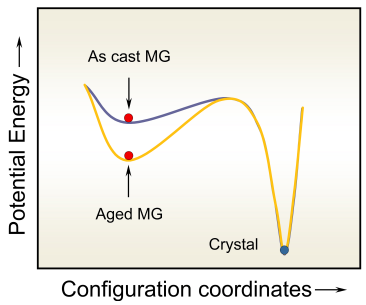

Figure 6 Schematic diagram of the potential energy landscape for as-cast and aged MG system.

enthalpy overshoot at the onset of crystallization, followed by delayed crystallization.

In terms of the potential energy landscape, the annealed MG is located in a much lower energy basin, as schematic plotted in Figure 6. Upon reheating, the fast-relaxing domains that are trapped in the low fictive temperature T_f state can start to regain enthalpy. Since the degree of annealing is high enough that the enthalpy is regained at higher temperatures. That is, shadow glass transition occurs at higher temperatures. The characteristic relaxation time for enthalpy relaxation is usually much shorter than the characteristic time for nucleation [23,39], i.e., crystallization starts to occur only after the completion of the shadow glass transition. At this point, the annealed MG crystallization faces a larger energy barrier. The energy barrier jump requires more external thermal energy. To overcome the energy barrier, it will crystallize at a higher temperature.

For MGs with good thermal stability, the glass transition can be exposed at ordinary heating rates. After annealing, MGs have a certain thermal history and show the shadow glass transition or enthalpy overshoot on DSC curves [8]. The thermal history exists only in the glassy state. When the glass transition occurs, the

thermal history disappears [40,41] and thus does not affect the crystallization. In the case of MGs with poor thermal stability, the glass transition is not exposed, and there is no supercooled liquid region. The glass state with thermal history is directly transformed into the crystallization processes. The thermal history is not eliminated by the glass transition, thus affecting the crystallization.

To substantiate our arguments, we have conducted a molecular dynamic simulation. As sketched in Figure 7A, we first generated $Al_{98}Sm_2$ MG by quenching an $Al_{98}Sm_2$ liquid from 1000 to 1 K at 10^{12} K/s at zero pressure. Then, the glass was heated to 1000 K at a heating rate of 10^{10} K/s (heating 1), and the potential energy dropped suddenly around 460 K, which indicates that the glass has crystallized. For a better understanding of the behavior of annealing delayed crystallization, we annealed the quenched glass (10^{12} K/s cooling) at 400 K for a long time, the potential energy of the glass slowly decreased as annealing took place. Next, we heated the annealed MG at 10^{10} K/s to 810 K (heating 2), the potential energy increases dramatically as the temperature rises. It is noteworthy that the annealed MG did not crystallize upon heating. Thus, the simulations reproduce the experiment findings.

Figure 7B shows the extracted three-dimensional (3D) atomic configurations when heated to 600 K. The dimensions of the glasses are about 5.5 nm × 5.5 nm × 5.5 nm, containing 9088 atoms. For the direct heating of quenched glass (heating 1), a large amount of FCC and a small amount of HCP crystalline phases have already precipitated, whereas the annealed MG remains amorphous state at 600 K (heating 2).

Figure 7C quantifies the fraction (N_{str}/N) of atoms in string-like configurations (N_{str}) to the total number of atoms (N = 9088) as functions of temperature. Figure 7D shows 3D string-like configurations at T = 380 K and time intervals δt = 100 ps. As can be seen from Figure 7C and D, the annealed MG has fewer atoms in string-like configurations when heated. Several studies have suggested that string-like motions could be the origin of β relaxation in MGs [42–45]. That is, for annealed MG, β relaxation is suppressed.

We note that our findings are not limited to MGs. Cheng *et al*. [24] reported that in PCMs, suppression of β relaxation sharply slowed down the crystallization rate, thereby enhancing the stability of the amorphous material. Earlier studies showed that the shadow glass transition arises from the β relaxation [25,34]. For the annealed MG, both the shadow glass transition and crystallization are shifted to high temperatures upon annealing. This implies that the mechanism of slowed crystallization could be the suppression of the β relaxation.

Pries *et al*. [33] compared the PCM $Ge_2Sb_2Te_5$ with chalcogenides such as GeSe, as shown in samples 13 and 14 in Table 1. After annealing at 388 K ($0.89T_p$) for 1 h, $Ge_2Sb_2Te_5$ shows an increased crystallization temperature similar to that of MGs studied here. The crystallization rate of GeSe does not change after annealing at 438 K ($0.78T_g$) for 1 h. While PCMs have poor glass formation ability [46,47] and usually crystallize before the glass transition, the chalcogenide GeSe is a non-PCM with a better glass forming ability and exhibits a glass transition [48]. Annealing has not shifted the crystallization temperature of GeSe. These observations are similar to that of MGs. In this context, the increased crystallization temperatures after annealing in PCMs is likely to be also related to a shifted shadow glass transition due to a suppressed β relaxation.

The emergence of shadow glass transition and enthalpy overshoot are all heat absorption processes, $dq > 0$. From the Clausius formula for entropy $dS \geqslant dq/T$, we may find $dS > 0$. This is an entropy-increasing process corresponding to more disorder in MGs. We can modulate the shadow glass transition to achieve delayed nucleation events and improve the stability of the glass.

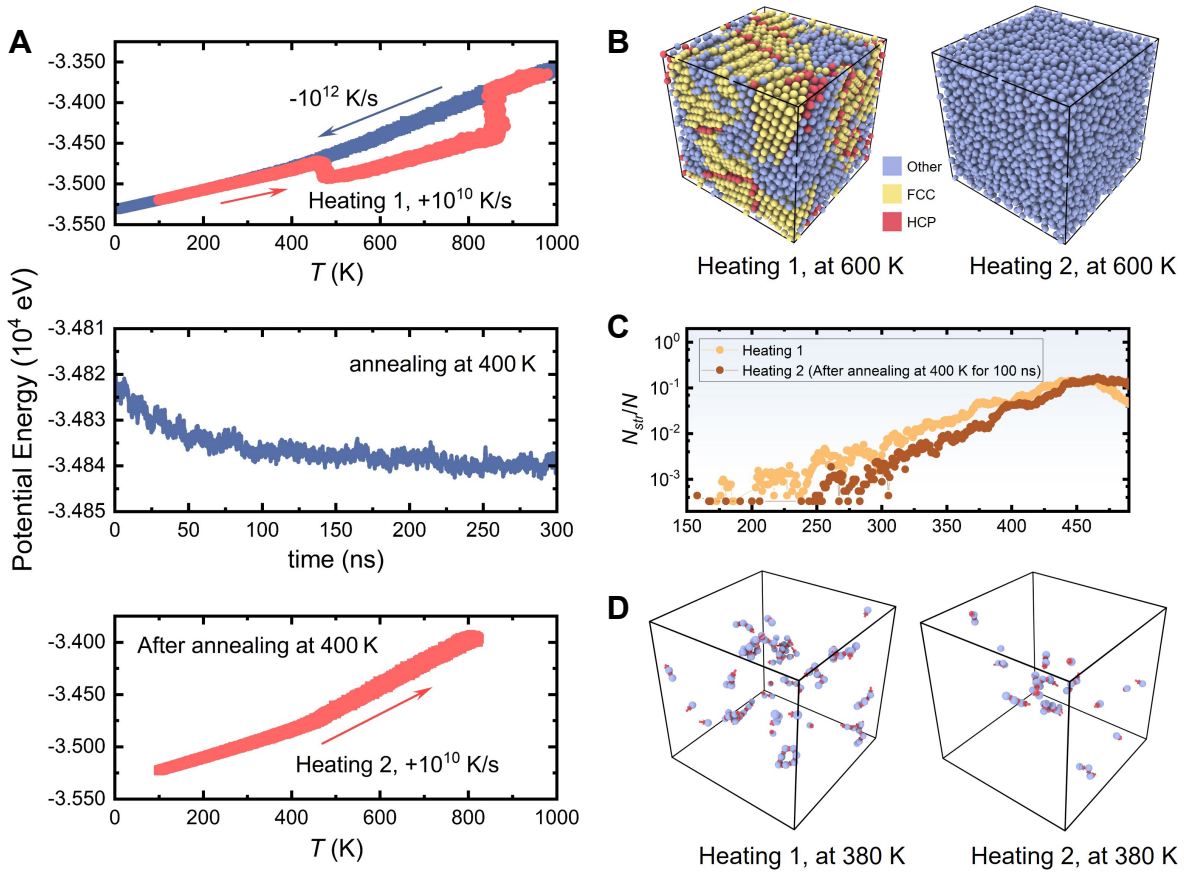

Figure 7 Molecular dynamics simulation of $Al_{98}Sm_2$ MG. (A) Potential energy versus temperature or time. (B) Three-dimensional (3D) view of atomic configurations, T = 600 K. (C) Dynamic evolution of string-like motions. The plot shows the fraction of atoms in string-like configurations to the total number of atoms as a function of temperature for quenched and annealed MG as indicated. (D) 3D view of the string-like configurations, T = 380 K and δt = 100 ps.

METHODS

Sample preparation

Twelve different MGs made by melt-spinning technology were selected for the experiments. They can be broadly classified into two categories. One shows a clear glass transition at normal heating rates, and the other crystallizes directly without the glass transition. Table 1 lists their chemical compositions. First, Y-based, La-based, Al-based, and Ce-based alloy ingots were fabricated by melting high-purity elements (with a purity of ⩾99.99 at%) in an arc-melting furnace under a Ti-gettered argon atmosphere. Each ingot was remelted five times to provide uniformity of composition. For the different alloy compositions, the alloy ingot was remelted using RF induction. The melt was sprayed onto the surface of individual copper rolls at a certain speed, from which amorphous ribbons were prepared. The amorphous properties of these ribbons were subsequently characterized by X-ray diffraction (XRD, Bruker D2 phaser) and DSC (Mettler Toledo DSC 3). Next, ribbons were subjected to annealing treatment. A short annealing time can be performed directly in the DSC instrument under the protection of a nitrogen atmosphere at 50 mL/min. Longer annealing treatments are performed in a chamber sintering furnace. To prevent oxidation of the sample, the tube

is sealed by evacuating the quartz tube using a mechanical pump, followed by high-purity argon gas, and finally sealed.

Calorimetry measurement

This experiment was carried out by flash differential scanning calorimetry (Mettler Toledo Flash DSC 2+). Based on the high heating rates of Flash DSC, the MGs were heated continuously under an 80 mL/min argon atmosphere, and the corresponding heat flow curves were obtained. Samples of FSC were obtained by micro-cutting under an optical microscope, and the produced samples were subsequently transferred to the sensitive area at the sample end of the sensor by electrostatic brushes under an optical microscope for measurement. To ensure the accuracy of the experimental data, all FSC experimental samples were sized as uniformly as possible, while baseline measurements were performed. Prior to testing the samples, FSC chip sensors were pretreated and calibrated according to the manufacturer's recommendations. Both low-temperature (UFS1) and high-temperature (UFH1) sensor types were used in this experiment.

Simulation details

An open-source molecular dynamics code, LAMMPS, was used for the simulation. Our model system contains N = 9088 atoms with the composition of $Al_{98}Sm_2$ MG. The glassy samples were prepared by quenching a liquid from 1000 to 1 K at 10^{12} K/s. The external pressure was adjusted to around zero. Periodic boundary conditions were applied for all the simulations.

Data availability

All the experimental data are included in the article and Supplementary Information. Simulation data can be requested from the corresponding author.

Acknowledgements

The computational work was carried out on the public computing service platform provided by the Network and Computing Center of Huazhong University of Science and Technology.

Funding

This work was supported by the National Thousand Young Talents Program of China, the National Natural Science Foundation of China (52071147 and 52201180), and the China Postdoctoral Science Foundation (2023T160241 and 2023M731176). S.W. thanks the support of Novo Nordisk Foundation (NNF21OC0071257).

Author contributions

H.B.Y., Q.Y. and H.R.Z. designed the work. H.B.Y., Q.Y., S.W. and Y.Z.Y. conceived the mechanism. H.R.Z. and Q.Y. fabricated the samples. H.R.Z. conducted the experiments. H.B.Y. performed the molecular dynamics simulation. H.R.Z., Y.Z.Y. and H.B.Y. wrote the manuscript with input from S.W..

Conflict of interest

The author declares no conflict of interest.

Supplementary information

The supporting information is available online at https://doi.org/10.1360/nso/20230064. The supporting materials are published as submitted, without typesetting or editing. The responsibility for scientific accuracy and content remains entirely with the authors.

References

1 Debenedetti PG, Stillinger FH. Supercooled liquids and the glass transition. *Nature* 2001; **410**: 259–267.
2 Dyre JC. Colloquium: The glass transition and elastic models of glass-forming liquids. *Rev Mod Phys* 2006; **78**: 953–972.
3 Zeng Q, Sheng H, Ding Y, *et al.* Long-range topological order in metallic glass. *Science* 2011; **332**: 1404–1406.
4 Ma E. Tuning order in disorder. *Nat Mater* 2015; **14**: 547–552.
5 Perepezko JH. Nucleation-controlled reactions and metastable structures. *Prog Mater Sci* 2004; **49**: 263–284.
6 Richert R. Physical aging and heterogeneous dynamics. *Phys Rev Lett* 2010; **104**: 085702.
7 Berthier L, Biroli G. Theoretical perspective on the glass transition and amorphous materials. *Rev Mod Phys* 2011; **83**: 587–645.
8 Zheng Q, Zhang Y, Montazerian M, *et al.* Understanding glass through differential scanning calorimetry. *Chem Rev* 2019; **119**: 7848–7939.
9 Qiao JC, Wang Q, Pelletier JM, *et al.* Structural heterogeneities and mechanical behavior of amorphous alloys. *Prog Mater Sci* 2019; **104**: 250–329.
10 Wang W. Roles of minor additions in formation and properties of bulk metallic glasses. *Prog Mater Sci* 2007; **52**: 540–596.
11 Ediger MD. Perspective: Highly stable vapor-deposited glasses. *J Chem Phys* 2017; **147**: 210901.
12 Swallen SF, Kearns KL, Mapes MK, *et al.* Organic glasses with exceptional thermodynamic and kinetic stability. *Science* 2007; **315**: 353–356.
13 Kearns KL, Swallen SF, Ediger MD, *et al.* Influence of substrate temperature on the stability of glasses prepared by vapor deposition. *J Chem Phys* 2007; **127**: 154702.
14 Guo Y, Morozov A, Schneider D, *et al.* Ultrastable nanostructured polymer glasses. *Nat Mater* 2012; **11**: 337–343.
15 Yu HB, Luo Y, Samwer K. Ultrastable metallic glass. *Adv Mater* 2013; **25**: 5904–5908.
16 Singh S, Ediger MD, de Pablo JJ. Ultrastable glasses from in silico vapour deposition. *Nat Mater* 2013; **12**: 139–144.
17 Gujral A, Gómez J, Jiang J, *et al.* Highly organized smectic-like packing in vapor-deposited glasses of a liquid crystal. *Chem Mater* 2017; **29**: 849–858.
18 Luo P, Cao CR, Zhu F, *et al.* Ultrastable metallic glasses formed on cold substrates. *Nat Commun* 2018; **9**: 1389.
19 Yu HB, Tylinski M, Guiseppi-Elie A, *et al.* Suppression of β relaxation in vapor-deposited ultrastable glasses. *Phys Rev Lett* 2015; **115**: 185501.
20 Qiao JC, Pelletier JM. Isochronal and isothermal crystallization in $Zr_{55}Cu_{30}Ni_5$ Al10 bulk metallic glass. *Trans Nonferrous Met Soc China* 2012; **22**: 577–584.
21 Venkataraman S, Rozhkova E, Eckert J, *et al.* Thermal stability and crystallization kinetics of Cu-reinforced $Cu_{47}Ti_{33}Zr_{11}Ni_8Si_1$ metallic glass composite powders synthesized by ball milling: The effect of particulate reinforcement. *Intermetallics* 2005; **13**: 833–840.
22 Ma CF, Wang F, Huang P, *et al.* Hillock growth in CuZr metallic glass. *Thin Solid Films* 2015; **589**: 681–685.
23 Zhao Y, Shang B, Zhang B, *et al.* Ultrastable metallic glass by room temperature aging. *Sci Adv* 2022; **8**: eabn3623.
24 Cheng Y, Yang Q, Wang J, *et al.* Highly tunable β-relaxation enables the tailoring of crystallization in phase-change materials. *Nat Commun* 2022; **13**: 7352.
25 Yang Q, Peng SX, Wang Z, *et al.* Shadow glass transition as a thermodynamic signature of β relaxation in hyper-quenched metallic glasses. *Natl Sci Rev* 2020; **7**: 1896–1905.

26 Pan J, Wang YX, Guo Q, *et al.* Extreme rejuvenation and softening in a bulk metallic glass. *Nat Commun* 2018; **9**: 560.

27 Ketov SV, Sun YH, Nachum S, *et al.* Rejuvenation of metallic glasses by non-affine thermal strain. *Nature* 2015; **524**: 200–203.

28 Velikov V, Borick S, Angell CA. The glass transition of water, based on hyperquenching experiments. *Science* 2001; **294**: 2335–2338.

29 Hu L, Zhou C, Zhang C, *et al.* Thermodynamic anomaly of the sub-T_g relaxation in hyperquenched metallic glasses. *J Chem Phys* 2013; **138**: 174508.

30 Liu YH, Fujita T, Aji DPB, *et al.* Structural origins of Johari-Goldstein relaxation in a metallic glass. *Nat Commun* 2014; **5**: 3238.

31 Inoue A, Masumoto T, Chen HS. Enthalpy relaxation behaviour of metal-metal (Zr-Cu) amorphous alloys upon annealing. *J Mater Sci* 1985; **20**: 4057–4068.

32 Yue Y, Angell CA. Clarifying the glass-transition behaviour of water by comparison with hyperquenched inorganic glasses. *Nature* 2004; **427**: 717–720.

33 Pries J, Wei S, Wuttig M, *et al.* Switching between crystallization from the glassy and the undercooled liquid phase in phase change material $Ge_2Sb_2Te_5$. *Adv Mater* 2019; **31**: 1900784.

34 Yu HB, Wang WH, Bai HY, *et al.* The β-relaxation in metallic glasses. *Natl Sci Rev* 2014; **1**: 429–461.

35 Yue YZ. Characteristic temperatures of enthalpy relaxation in glass. *J Non-Crystalline Solids* 2008; **354**: 1112–1118.

36 Gao S, Koh YP, Simon SL. Calorimetric glass transition of single polystyrene ultrathin films. *Macromolecules* 2013; **46**: 562–570.

37 Koh YP, Grassia L, Simon SL. Structural recovery of a single polystyrene thin film using nanocalorimetry to extend the aging time and temperature range. *ThermoChim Acta* 2015; **603**: 135–141.

38 Gao Y, Zhao B, Vlassak JJ, *et al.* Reprint of: Nanocalorimetry: Door opened for *in situ* material characterization under extreme non-equilibrium conditions. *Prog Mater Sci* 2021; **120**: 100819.

39 Androsch R, Schick C, Schmelzer JWP. Sequence of enthalpy relaxation, homogeneous crystal nucleation and crystal growth in glassy polyamide 6. *Eur Polym J* 2014; **53**: 100–108.

40 Evenson Z, Gallino I, Busch R. The effect of cooling rates on the apparent fragility of Zr-based bulk metallic glasses. *J Appl Phys* 2010; **107**: 123529.

41 Zhao R, Jiang HY, Luo P, *et al.* Reversible and irreversible β-relaxations in metallic glasses. *Phys Rev B* 2020; **101**: 094203.

42 Yu HB, Yang MH, Sun Y, *et al.* Fundamental link between β relaxation, excess wings, and cage-breaking in metallic glasses. *J Phys Chem Lett* 2018; **9**: 5877–5883.

43 Zhou ZY, Sun Y, Gao L, *et al.* Fundamental links between shear transformation, β relaxation, and string-like motion in metallic glasses. *Acta Mater* 2023; **246**: 118701.

44 Gao L, Sun Y, Yu HB. Mobility percolation as a source of Johari-Goldstein relaxation in glasses. *Phys Rev B* 2023; **108**: 014201.

45 Yu HB, Richert R, Samwer K. Structural rearrangements governing Johari-Goldstein relaxations in metallic glasses. *Sci Adv* 2017; **3**: e1701577.

46 Salinga M, Carria E, Kaldenbach A, *et al.* Measurement of crystal growth velocity in a melt-quenched phase-change material. *Nat Commun* 2013; **4**: 2371.

47 Weber H, Orava J, Kaban I, *et al.* Correlating ultrafast calorimetry, viscosity, and structural measurements in liquid GeTe and $Ge_{15}Te_{85}$. *Phys Rev Mater* 2018; **2**: 093405.

48 Wei S, Evenson Z, Stolpe M, *et al.* Breakdown of the Stokes-Einstein relation above the melting temperature in a liquid phase-change material. *Sci Adv* 2018; **4**: eaat8632.